molecules

MDPI

Article

Revealing the Mechanism of Porous Graphene in Styrene-Butadiene-Styrene/Crumb Rubber-Modified Asphalt: A Molecular Dynamics Study

Yilin Huang [1,2,*], Weijie Jiang [1], Heyang Wu [1], Zhiheng Wu [3], Shuqi Hu [1,4] and Linqiang Mo [5]

[1] Guangxi University Engineering Research Center of Advanced Technologies and Materials Applicated in Transportation, College of Traffic and Transportation, Nanning University, Nanning 530200, China
[2] Guangxi Key Laboratory of International Join for China-ASEAN Comprehensive Transportation, Nanning 530200, China
[3] Intelligent Transportation System Research Center, Southeast University, Nanjing 211189, China
[4] Nanning Engineering Technology Research Center for Power Transmission System of New Energy Vehicle, College of Traffic and Transportation, Nanning University, Nanning 530200, China
[5] School of Road and Bridge Engineering, Guangxi Transport Vocational and Technical College, Nanning 530023, China
* Correspondence: huangyilin@unn.edu.cn

Abstract

Clarifying the interaction between graphene and styrene–butadiene–styrene block copolymer (SBS)/crumb rubber (CR)-modified asphalt is essential for applying graphene-modified asphalt. Therefore, the mechanical properties of SBS/CR-modified asphalt incorporating different dosages of porous graphene (PG) were investigated via molecular dynamics simulation to elucidate PG's role and mechanism in the SBS/CR/asphalt blend system. The results demonstrate that high-temperature elasticity and low-temperature flexibility of SBS/CR-modified asphalt were most effectively improved at a PG content of 2%. Compared with SBS/CR-modified asphalt, modified asphalt with 2% PG exhibits a 30.8% increase in modulus at 353 K, and the diffusion coefficient of SBS molecules at 273 K is increased by 101.6%. These improvements are attributed to the optimal electrostatic attraction between PG and CR molecules at this content, while SBS has good extensibility, acting as a 'bridge' connecting the CR molecules, effectively reducing the pores in the modified asphalt, improving their cohesion, and enhancing the high-temperature performance. Additionally, the outstanding flexibility of SBS at low temperatures within the network structure formed by PG boosts the low-temperature crack resistance of modified asphalt. The findings of this study provide a new perspective on modified asphalt blend systems.

Keywords: porous graphene; modified asphalt blend system; interaction; mechanical properties; molecular dynamics simulation

Check for updates

Academic Editor: Chan Kyung Kim

Received: 26 September 2026
Revised: 31 October 2026
Accepted: 8 November 2026
Published: 19 November 2026

Copyright: © 2026 by the authors. Licensee MDPI, Basel, Switzerland. This article is an open access article distributed under the terms and conditions of the Creative Commons Attribution (CC BY) license.

1. Introduction

Asphalt binder has been widely used in road paving in civil engineering [1]. Its mechanical properties, which vary with temperature, are a critical factor directly affecting the service performance of pavements [2]. At present, asphalt modified with polymer modifiers, like rubber, styrene–butadiene–styrene (SBS), and ethylene–vinyl acetate (EVA), is commonly used for high-grade pavement because these polymers, with their long chains and high molecular weight, provide extra shear resistance and good thermal stability [3–5]. Among these polymer modifiers, crumb rubber not only improves asphalt performance

but also promotes the recycling of waste tires and helps mitigate 'black pollution' [6]. However, in such multi-phase blend systems, there is a substantial difference in molecular weight between polymer molecules and base asphalt, readily inducing phase separation, thereby deteriorating the mechanical performance of modified asphalt [7,8]. Therefore, improving the multi-phase compatibility of asphalt is an effective approach to enhancing its thermo-mechanical performance.

Use of sulfur-containing stabilizers is a traditional method to promote cross-linking between polymer molecules and improve the stability of the asphalt multi-phase blend system [9]. However, the sulfur compounds can evaporate and release gases with a strong, irritating odor during high-temperature mixing, posing risks to human health [10]. In addition, multi-component polymer composite-modified asphalt also demonstrated good mechanical performance and stability [11]. In recent years, researchers have explored the use of nanomaterials, such as nanoclay [12], nano-silica [13], nano-TiO_2 [14], nano-calcium carbonate [15], and carbon materials [16], to improve the compatibility of asphalt multi-phase systems and reduce the use of sulfur-containing stabilizers. Among these nanomaterials, graphene and its derivatives have attracted considerable attention owing to their unique layered structure, excellent mechanical strength, barrier properties, and high specific surface area [17,18]. To date, various graphene-modified asphalt systems have been investigated, including graphene/asphalt binary systems and graphene/polymer/asphalt ternary systems. For instance, in the research on the system of graphene/polymer/asphalt, Li et al. [19] incorporated graphene oxide (GO) powder and GO dispersions into SBS-modified asphalt separately and found that GO significantly improved the viscosity, storage stability, and recovery ability of the modified asphalt; moreover, the dispersion outperformed the powder, achieving a recovery rate of 38.7% at 0.1 kPa. Wang et al. [20] blended graphene into SBS-modified asphalt and reported that at a dosage of 0.65% graphene markedly enhanced rutting resistance while exerting little influence on fatigue or thermal cracking resistance. Adnan et al. [21] prepared graphene/tire rubber powder (TRP) composite-modified asphalt, which alleviated phase separation in rubber-modified asphalt, improved its compatibility, and enhanced its rutting resistance, aging resistance, fatigue performance, and low-temperature performance. Similarly, Li et al. [22] employed GO and rubber powder (RP) as composite modifiers for base asphalt; the results showed that at 0.1 kPa and 64 °C, the addition of GO increased the recovery rate of RP-modified asphalt by 21.2%, reduced the non-recoverable creep compliance by 31.3%, and significantly improved creep recovery. These experimental studies confirm that incorporating graphene can improve the compatibility between polymers and asphalt and enhance the performance of composite-modified asphalt.

Regarding the mechanism of graphene composite polymer-modified asphalt, some researchers suggest that adding graphene affects the dispersion of polymer phase in the asphalt matrix, resulting in a more uniform distribution of SBS [23]. Hu et al. [24] further proposed that introducing graphene strengthens the binding energy between rubber powder and the non-polar fractions of asphalt (i.e., saturates and aromatics fractions), thereby promoting the swelling of crumb rubber in asphalt. Consistently, Huo et al. [25] demonstrated that graphene enhances the bonding between rubber and the light components of asphalt, facilitating the absorption of light components by rubber, stabilizing the rubber–resin interface, and ultimately improving the compatibility between rubber and asphalt as well as the mechanical performance of the blend. Although progress has been made on the graphene/polymer/asphalt ternary system, the underlying mechanism of graphene in such modified asphalt blend systems remains unclear, which restricts the application and development of multi-phase blended asphalt.

In this work, we performed molecular dynamics (MD) simulations to investigate the reinforcement mechanism of PG/SBS/CR composite-modified asphalt blend systems. We first adopted SBS/CR-modified asphalt as the control group and constructed modified asphalt models with different PG contents. We then evaluated the high- and low-temperature mechanical properties of these models through shear and tensile simulations; analyzed parameters such as the diffusion coefficient, molecular distribution, and cohesive energy in detail; and finally elucidated the role of PG in the SBS/CR-modified asphalt blend system by analyzing the atomic bonding within the models.

2. Results and Discussion

2.1. High-Temperature Mechanical Properties of PG Composite SBS/CR-Modified Asphalt

The high-temperature performance of PG-modified SBS/CR asphalt was examined at different PG contents. The pink bars in Figure 1 present the shear modulus of the asphalt models at 353 K. The shear modulus increases gradually with increasing PG content and reaches its maximum at a PG content of 2%. Specifically, the shear modulus of SBS/CR MA is 0.26 GPa, whereas that of 2% G-SBS/CR MA reaches 0.34 GPa, a significant increase of 30.8% relative to SBS/CR MA. At a higher PG content (3%), however, the mechanical performance decreases, possibly because excessive PG aggregates and thereby weakens the cohesive force between molecules. In terms of molecular mobility, 2%G-SBS/CR MA exhibits the slowest diffusion rate (0.022), which is 24.14% lower than that of SBS/CR MA (0.029). This phenomenon may be attributed to the appropriate PG dosage, which not only allows PG to disperse and form a network structure but also enhances the interfacial interactions and cohesive energy of the asphalt molecules.

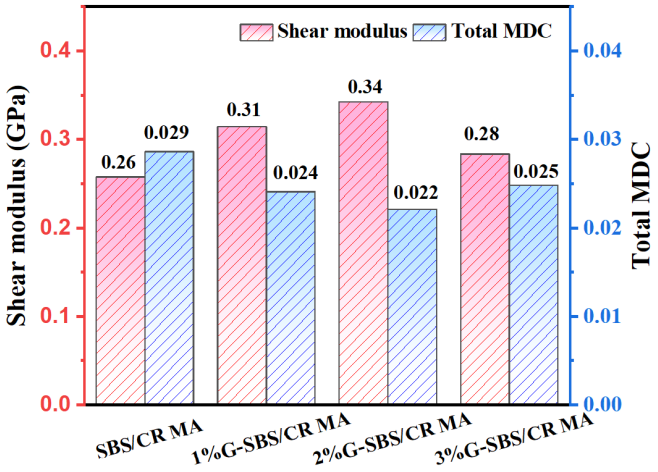


Figure 1. Comparison of mechanical properties and total diffusivity of PG/SBS/CR-modified asphalt models with different content.

To further investigate the changes in molecular motion, the molecule diffusion coefficients (MDCs) of each component in the modified asphalt models were analyzed, as shown in Figure 2. At 353 K, the MDCs of SBS, CR, and the four asphalt fractions increase with PG content up to 2% and then decrease. For the 2% G-SBS/CR MA, the MDC of SBS molecules is 34.8% lower than that of SBS/CR MA, while that of CR molecules decreases by 29.1%, indicating that an appropriate PG content can minimize molecular diffusion and thereby enhance the high-temperature deformation resistance of SBS/CR MA. The four asphalt fractions exhibit a similar trend to SBS and CR, with reductions of approximately 20–30% relative to SBS/CR MA. These results indicate that 2% G-SBS/CR MA markedly reduces the molecular mobility of the modified asphalt and, thus, improves its mechanical properties.

Notably, the reduction in diffusion is most pronounced for SBS molecules, highlighting the important role of SBS in this complex system.

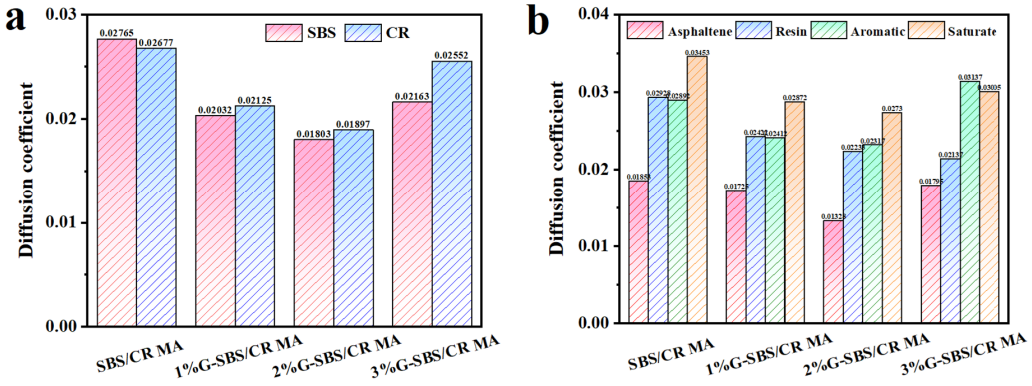


Figure 2. Comparison of diffusion coefficients of each component in PG/SBS/CR-modified asphalt models with different PG contents: (**a**) SBS and CR, (**b**) the four asphalt fractions.

To explore the relationship between molecular mobility and molecular distribution in the asphalt models, the radius of gyration (Rg) was adopted to characterize the compactness of the molecular system and the extensibility of the polymer, reflected in the dynamic variations in molecular volume and shape. The lower the peak position of Rg for a molecular system, the more compact the system; the narrower the peak width, the more readily the molecular branches extend spatially and wrap around the surrounding molecules. Figure 3a presents the Rg of SBS molecules in the models. With the addition of PG, the Rg peak shifts to a higher value while its width decreases, indicating that PG facilitates the dispersion and extension of SBS molecules. This suggests that SBS in such a structure may more easily bridge dispersed CR particles. Nevertheless, when the PG content reaches 3%, the Rg peak of SBS shifts back to a lower position and broadens, implying that excessive PG may promote aggregation and hinder the uniform dispersion of SBS. Interestingly, in 2% G-SBS/CR MA, the SBS peak width is narrower than in 1% G-SBS/CR MA, indicating that the addition of 2% PG further facilitates the extension of SBS and improves its stretchability. In addition, Figure 3b demonstrates that the Rg peak of CR molecules shifts to a higher value and that molecular compactness decreases with increasing PG content, indicating that PG promotes the swelling of CR, particularly at PG contents of 2% and 3%.

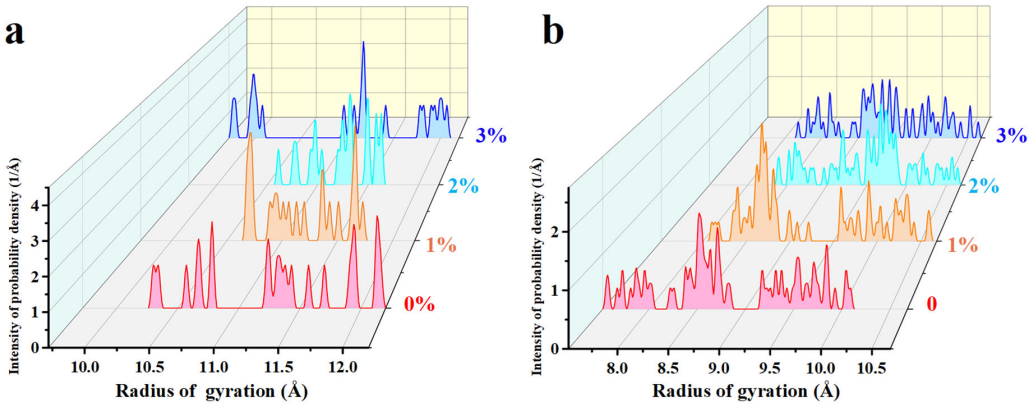


Figure 3. Rg distributions of components in PG/SBS/CR-modified asphalt models with different contents: (**a**) SBS and (**b**) CR.

The Rg of the four asphalt fractions in the modified asphalt system was further explored to elucidate their structural distribution. As shown in Figure 4a, the Rg peak of asphaltenes

decreases with increasing PG content, indicating a denser distribution of asphaltenes. Notably, the asphaltenes in 2% G-SBS/CR MA exhibit a narrow peak between 5.25 and 5.75 Å, suggesting that a PG content of 2% may confer an optimal packing density on the asphaltenes. In addition, the Rg peaks of resins, aromatics, and saturates also decrease after the addition of PG (Figure 4b–d). These results indicate that PG can enhance the overall compactness of the SBS/CR-modified asphalt system.

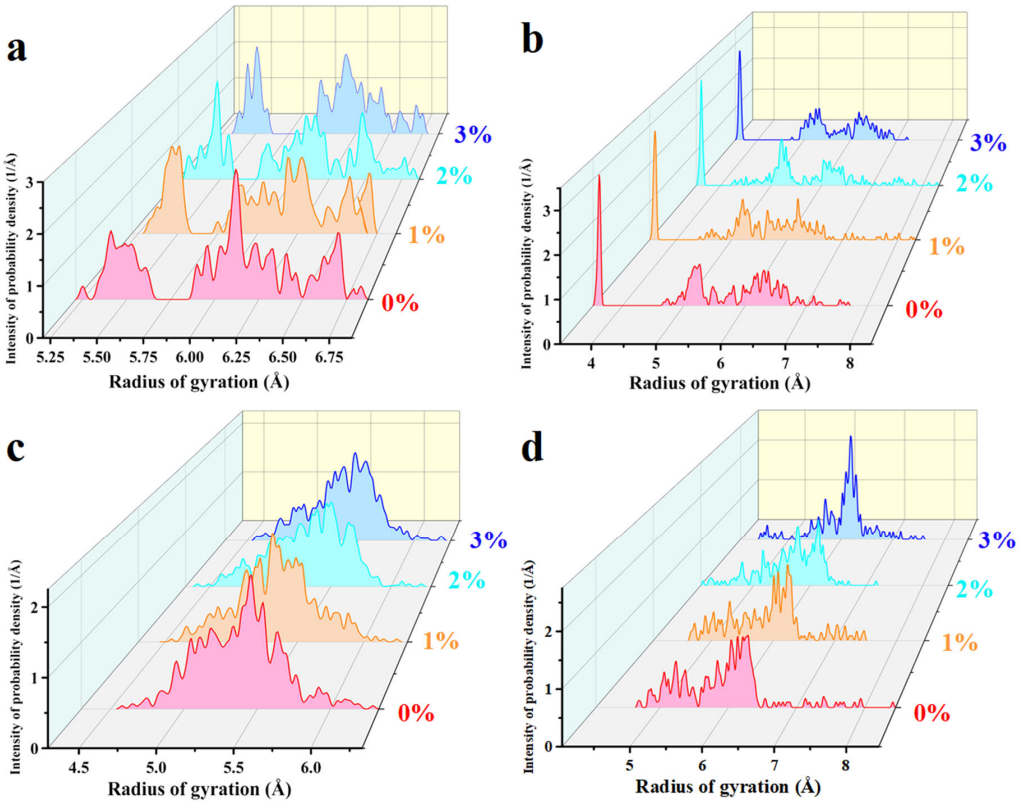


Figure 4. Rg distributions of each component in PG/SBS/CR-modified asphalt models with different PG contents: (**a**) asphaltenes, (**b**) resins, (**c**) aromatics, and (**d**) saturates.

Tensile simulations were performed to better understand the mechanical behavior of PG-composite SBS/CR-modified asphalt in complex systems. As shown in Figure 5a, the stress–strain curves of the modified asphalt model can be clearly divided into four stages: an elastic stage (strain 0~0.04), a yield stage (0.04~0.1), a strengthening stage (0.1~0.2), and a necking stage (>0.2). With the addition of PG, the tensile stress at a given strain increases. Compared with SBS/CR MA, 2% G-SBS/CR MA exhibits 17.7% higher stress in the elastic stage, 10% higher yield stress, and 7.3% higher maximum stress (Figure 5b). The 2% dosage, which is optimal, shows the highest stress in every stage, indicating the strongest cohesion and the greatest compactness of the PG composite-modified asphalt system.

To better understand the molecular movement during stretching, snapshots of the stretching process were analyzed. When the PG composite SBS/CR-modified asphalt model is stretched along the *X*-axis at 353 K, the lateral stretching distance decreases with increasing PG content (Figure 6a–d). Compared with SBS/CR MA, the stretching lengths of 1% G-SBS/CR MA, 2% G-SBS/CR MA, and 3% G-SBS/CR MA decrease by 0.93 Å, 2.09 Å, and 0.52 Å, respectively; notably, the value increases again at 3% PG content. This indicates that 2% G-SBS/CR MA exhibits the best resistance to high-temperature stress under the same stretching conditions, reflecting its optimal structural distribution and excellent cohesion. Furthermore, Figure 6e–h present the detailed distribution of PG, SBS,

CR, and asphalt molecules. As the PG content increases, the polymers are more inclined to form network structures; however, when the PG content is excessive, the interactions between PG and the asphalt molecules or polymers weaken, leading to local aggregation within the modified asphalt.

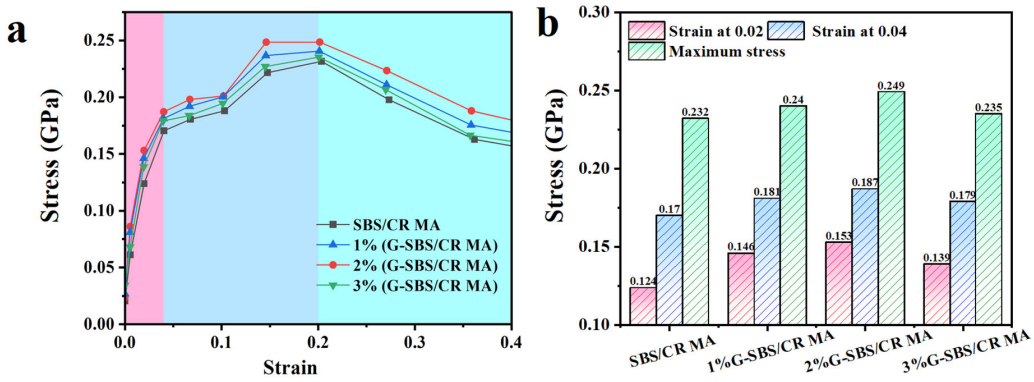


Figure 5. Tensile behavior of PG/SBS/CR-modified asphalt models with different PG contents: (**a**) stress–strain curves, (**b**) comparison of stresses at different stages.

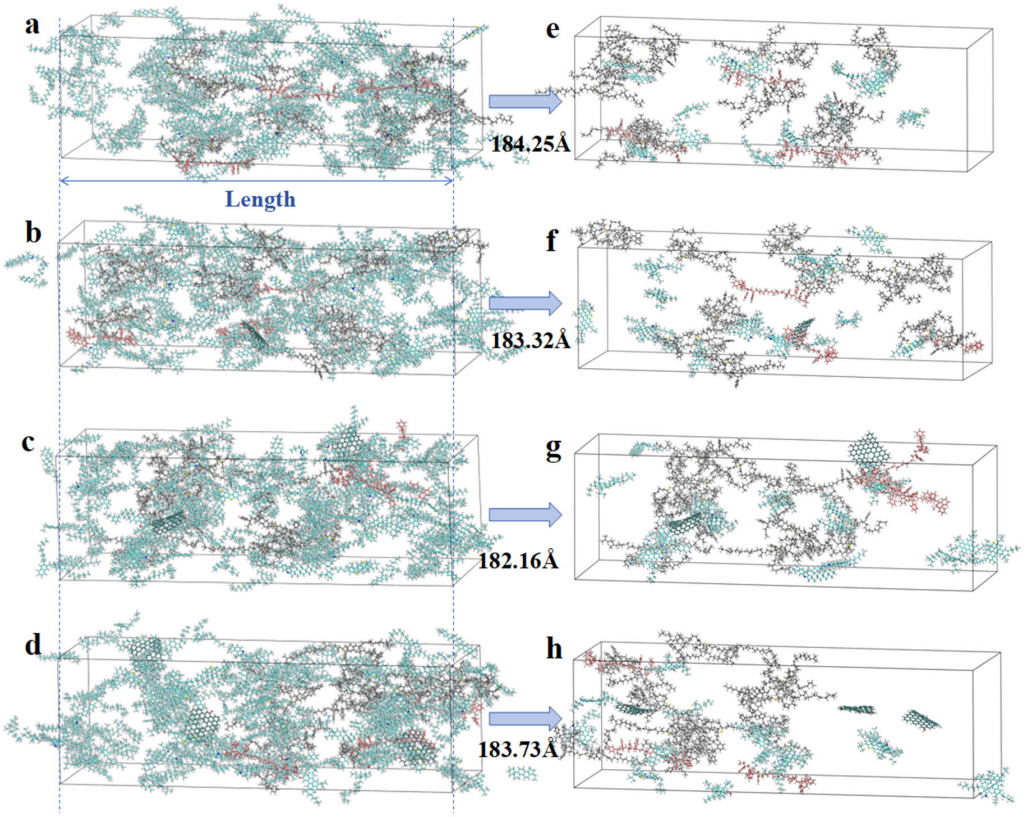


Figure 6. Snapshots of the tensile process of PG/SBS/CR-modified asphalt with different PG contents: before stretching (**a**) 0%, (**b**) 1%, (**c**) 2%, and (**d**) 3%, and after stretching (**e**) 0%, (**f**) 1%, (**g**) 2%, (**h**) 3%. (Red represents SBS, gray represents rubber, green represents asphalt, and cyan represents PG).

To further evaluate the compactness of SBS/CR-modified asphalt with different PG contents, the free volume of the model was analyzed. As shown in Figure 7, the free volume of modified asphalt decreases after the addition of PG. The free volume of SBS/CR MA accounts for 21.02% of the total volume, whereas the free volume ratios of 1% G-SBS/CR

MA, 2% G-SBS/CR MA, and 3% G-SBS/CR MA decrease to 20.24%, 20.12%, and 20.83%, respectively. Notably, 2% G-SBS/CR MA exhibits the lowest free volume, indicating that the active space available to the asphalt molecular chains is reduced and fewer asphalt molecules or monomer units can jump under shear stress. Meanwhile, a lower free volume corresponds to stronger cohesion and higher viscosity of modified asphalt, thereby improving its high-temperature mechanical properties.

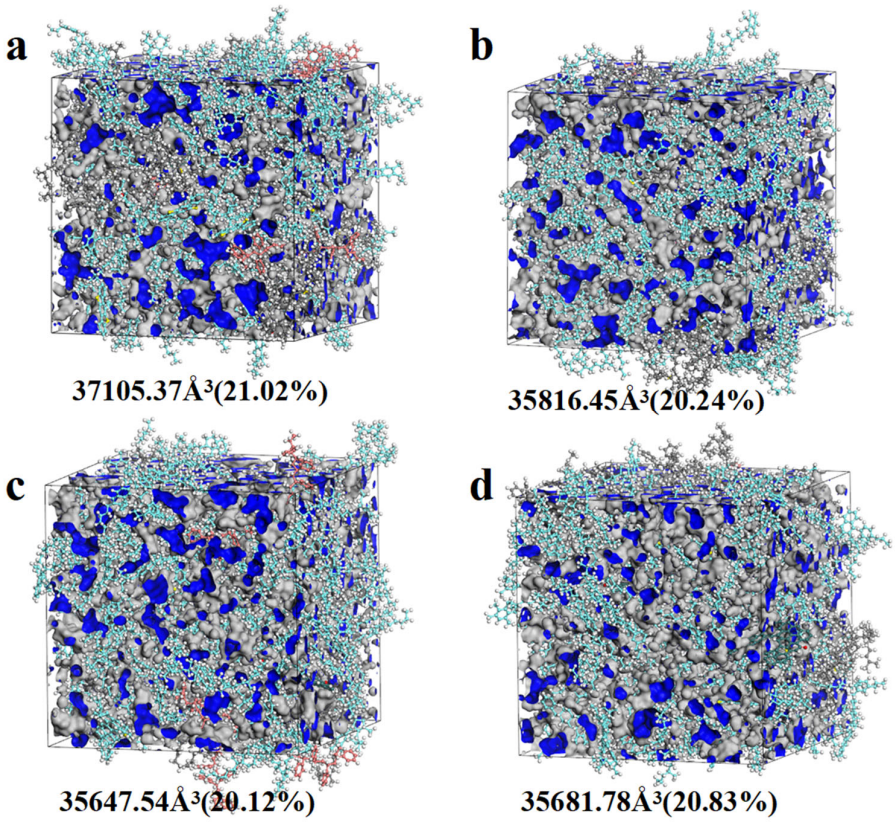


Figure 7. Free volume of PG/SBS/CR-modified asphalt models with different PG contents: (**a**) 0%, (**b**) 1%, (**c**) 2%, and (**d**) 3%.

Cohesive energy density (CED) effectively reflects the intermolecular attractive forces and evaluates the cohesive ability of a substance; a higher CED value indicates stronger binding ability. Table 1 lists the CED values of the modified asphalt models with different PG contents. In the molecular models, the van der Waals interactions are two orders of magnitude stronger than the electrostatic interactions, indicating that these asphalt systems are dominated by van der Waals forces. The CED of SBS/CR MA is 2.532×10^8 J/m^3, while the addition of 1%, 2%, and 3% PG increases the CED to 2.554×10^8 J/m^3, 2.581×10^8 J/m^3, and 2.537×10^8 J/m^3, respectively. These results suggest that PG can enhance the cohesive energy density of the SBS/CR-modified asphalt, thereby helping to improve its high-temperature performance.

To further elucidate the mechanism underlying the changes in cohesive energy from the perspective of molecular energy, the binding energies of different components in the asphalt models were analyzed. Table 2 lists the binding energies between PG and each asphalt component, together with a comparison of the binding energies between the polymers (SBS and CR) and the base asphalt. In the molecular models, the binding energy between PG and each component ranks as follows: aromatics > resins > saturates > asphaltenes, indicating that PG interacts strongly with the aromatics and resins in the blend system. In addition, the addition of PG increases the binding energy between the polymer molecules (SBS and

CR) and base asphalt; for the models with 1%, 2%, and 3% PG, the binding energies increase by 22.94 eV, 42.32 eV, and 13.81 eV, respectively. This illustrates that the PG dosage has a significant effect on the binding energy between the polymers and asphalt, with 2% PG yielding the highest value, which further strengthens the interactions among the SBS, CR, and asphalt molecules.

Table 1. Cohesive energy density of modified asphalt models with different PG contents.

Samples	Total ($J \cdot m^{-3}$)	van der Waals ($J \cdot m^{-3}$)	Electrostatic ($J \cdot m^{-3}$)
SBS/CR MA	2.532×10^8	2.371×10^8	1.867×10^6
1%G-SBS/CR MA	2.554×10^8	2.376×10^8	1.935×10^6
2%G-SBS/CR MA	2.581×10^8	2.380×10^8	1.984×10^6
3%G-SBS/CR MA	2.537×10^8	2.372×10^8	1.883×10^6

Table 2. Binding energies between components of the modified asphalt models.

	0 (eV)	1% (eV)	2% (eV)	3% (eV)
PG/Asphaltene	–	2.54	3.17	2.74
PG/Resin	–	10.34	11.28	10.49
PG/Saturate	–	20.42	21.07	20.58
PG/Aromatic	–	3.32	3.67	3.38
SBS/CR/Asphalt	1438.17	1461.11	1480.49	1451.98

2.2. Low-Temperature Mechanical Properties of PG Composite SBS/CR-Modified Asphalt

The low-temperature properties of PG composite SBS/CR-modified asphalt were evaluated via tensile simulation at 273 K. As shown in Figure 8a, the stress–strain curves can again be divided into four stages: elastic, yield, hardening, and necking. However, the curves of SBS/CR MA and 3% G-SBS/CR MA exhibit almost no hardening stage; the material fails immediately after yielding and enters the necking stage, suggesting that they are prone to brittleness and fracture at low temperatures. In contrast, the curves of 1% G-SBS/CR MA and 2% G-SBS/CR MA show a distinct hardening stage, indicating that these two samples do not fail immediately after yielding and, thus, possess better low-temperature toughness. Although their yield stresses are lower than those of SBS/CR MA and 3%G-SBS/CR MA, they can withstand higher fracture stresses at low temperatures. In particular, the maximum stress of 2% G-SBS/CR MA at a strain of 0.2 exceeds that of 1% G-SBS/CR MA, indicating that the low-temperature performance is optimal at a PG content of 2%. In addition, Figure 8b presents the MDC results of the SBS and CR molecules. The MDC of CR changes little after the addition of PG, whereas that of SBS increases remarkably: the SBS MDC in 2% G-SBS/CR MA is 101.6% higher than that in SBS/CR MA, the highest among all samples. This suggests that the improvement in low-temperature performance arises from the enhanced mobility (slippage) of SBS molecular chains at low temperatures.

To further understand the effect of PG contents on the stretching process at low temperatures from a molecular perspective, snapshots of the stretching process at 273 K were analyzed. As shown in Figure 9, the lateral stretching distance along the *X*-axis first increases and then decreases with increasing PG content. Compared with SBS/CR MA, the stretching lengths of 1% G-SBS/CR MA, 2% G-SBS/CR MA, and 3% G-SBS/CR MA increase by 2.25 Å, 2.5 Å, and 0.68 Å, respectively, with the 2% sample exhibiting the best toughness under the same stretching conditions and, thus, superior resistance to low-temperature cracking. In addition, Figure 9e–g present a detailed analysis of the distribution of PG, SBS, CR, and asphaltenes. Similarly to the observations at 353 K, the polymers in 1% G-SBS/CR

MA and 2% G-SBS/CR MA tend to form network structures, which enables SBS to diffuse effectively at low temperatures and thereby reduces the risk of low-temperature cracking.

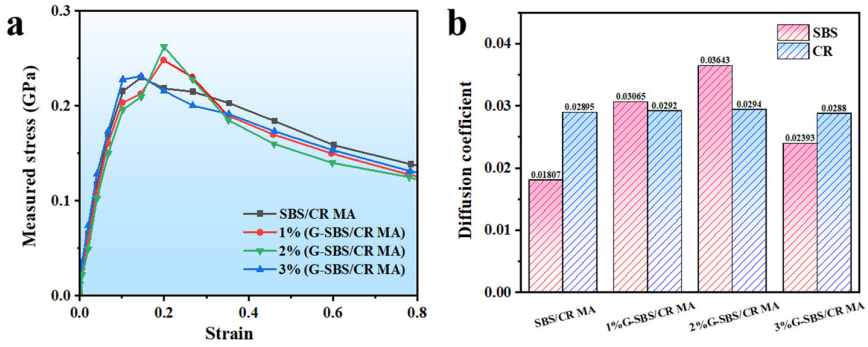


Figure 8. Comparison of (**a**) stress–strain curves and (**b**) diffusion coefficients of SBS/CR-modified asphalt with different PG dosages at 273 K.

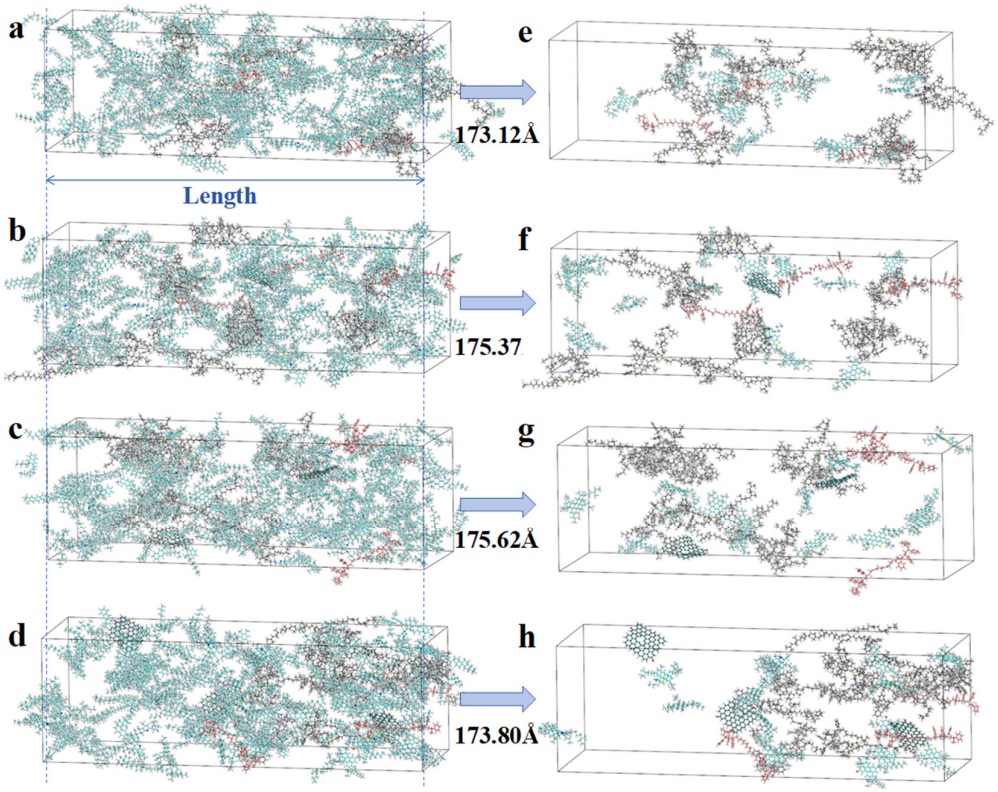


Figure 9. Snapshots of the tensile process of SBS/CR-modified asphalt models with different PG dosages at 273 K: before stretching (**a**) 0%, (**b**) 1%, (**c**) 2%, and (**d**) 3%, and after stretching (**e**) 0%, (**f**) 1%, (**g**) 2%, (**h**) 3%. (Red represents SBS, gray represents rubber, green represents asphalt, and cyan represents PG).

2.3. Analysis of the Mechanism of PG Content on SBS/CR-Modified Asphalt

To reveal the mechanism of PG/SBS/CR MA, a simplified model containing only SBS, CR, and PG molecules was constructed. As shown in Figure 10, CR molecules interact more strongly with PG, especially near the pores. The shortest CR-PG distances at PG contents of 1%, 2%, and 3% are 2.922 Å, 2.779 Å, and 2.936 Å, respectively, suggesting that 2% PG may induce the strongest CR-PG interaction and thereby promote the swelling of CR. In contrast, SBS does not directly interact with PG in this system; instead, the migration and distribution of SBS molecules are mainly governed by the electrostatic adsorption between PG and the

asphalt and CR molecules. Moreover, a single SBS chain can simultaneously entangle with rubber chains from different rubber particles, so the SBS molecules can act as physical bridges between the rubber particles, enabling stress transfer between the rubber phases.

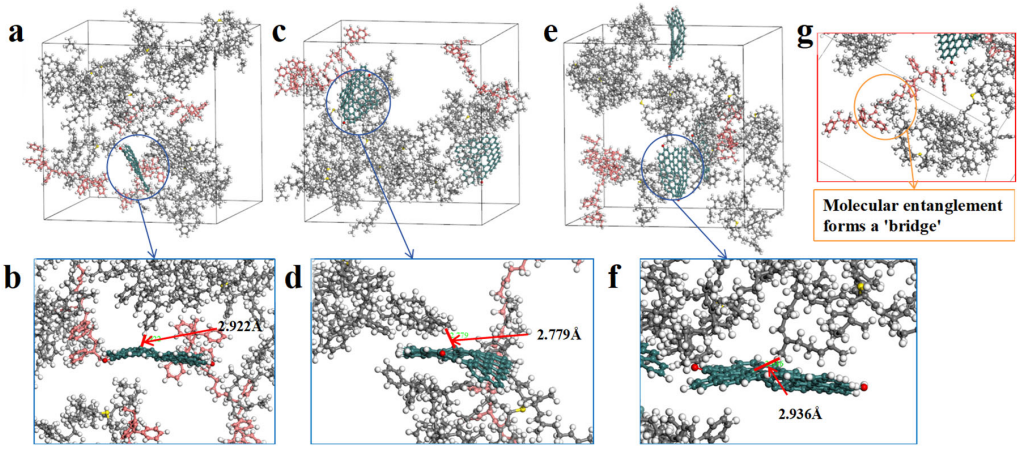


Figure 10. Molecular models and PG interface analysis of SBS/CR MA with different PG contents: (**a**,**b**) 1%, (**c**,**d**) 2%, (**e**,**f**) 3%, (**g**) entanglement between SBS and CR chains. (Red represents SBS, gray represents rubber, and cyan represents PG).

3. Molecular Dynamics Simulation Methods

3.1. Establishing the Asphalt Model

Asphalt is a complex organic mixture, and previous studies have widely used the four-component analysis method (SARA method) to separate it into four components: saturates (S), aromatics (AR), resins (R), and asphaltenes (A). In this work, four components of a twelve-molecule simulated asphalt proposed by Greenfield are used to build a matrix asphalt model [26], which contains molecules from all four SARA fractions. The saturates consist of $C_{35}H_{44}$ and $C_{31}H_{64}$; aromatics consist of $C_{28}H_{44}$ and $C_{29}H_{50}$; resins consist of $C_{34}H_{47}N$, $C_{29}H_{43}N$, $C_{18}H_{10}S$, $C_{44}H_{66}$, and $C_{30}H_{54}$; and asphaltenes consist of $C_{42}H_{54}O$, $C_{66}H_{83}N$, and $C_{51}H_{62}S$, which are shown in Figure 11a. Moreover, the content ratios of the four components in the matrix asphalt were determined through experiments, and the number of molecules of each component in the asphalt model was set accordingly (Figure 11b). The experimental results showed good consistency between the asphalt samples and the model in terms of composition, demonstrating the model's validity [27]. Then, using the Amorphous Cell module of Materials Studio (MS) software, version 2017 (Dassault Systèmes BIOVIA, San Diego, CA, USA), a 53 Å × 53 Å × 53 Å matrix asphalt model was constructed (Figure 11c).

In Figure 11d–f, the molecular cluster model of CR is made from natural rubber (NR), styrene–butadiene rubber (SBR), and sulfur cross-linking. SBS molecules are formed from styrene–butadiene–styrene polymerization, and the molecular model of PG is built with vacancy defects and oxygen-containing functional groups, based on the graphene prepared by Beibu Gulf Graphene Industry Technology Development Co., Ltd. (Nanning, China). This graphene has been thoroughly characterized and analyzed in previous reports [28]. Next, the SBS/CR-modified asphalt molecular models are built, and the components of the model include the base asphalt model, 20% CR cluster molecules, and 3% SBS molecules. Then, different contents of PG molecules (1%, 2%, and 3%) are added to the SBS/CR-modified asphalt model to obtain PG SBS/CR-modified asphalt. They are determined based on the percentage of the additive and the base asphalt by molecular weight. These four models are defined as SBS/CR MA, 1% G-SBS/CR MA, 2% G-SBS/CR MA, and 3% G-SBS/CR MA, respectively. In this work, each content was analyzed using a model at equilibrium, and we referred to the relevant literature regarding the model's authenticity [29].

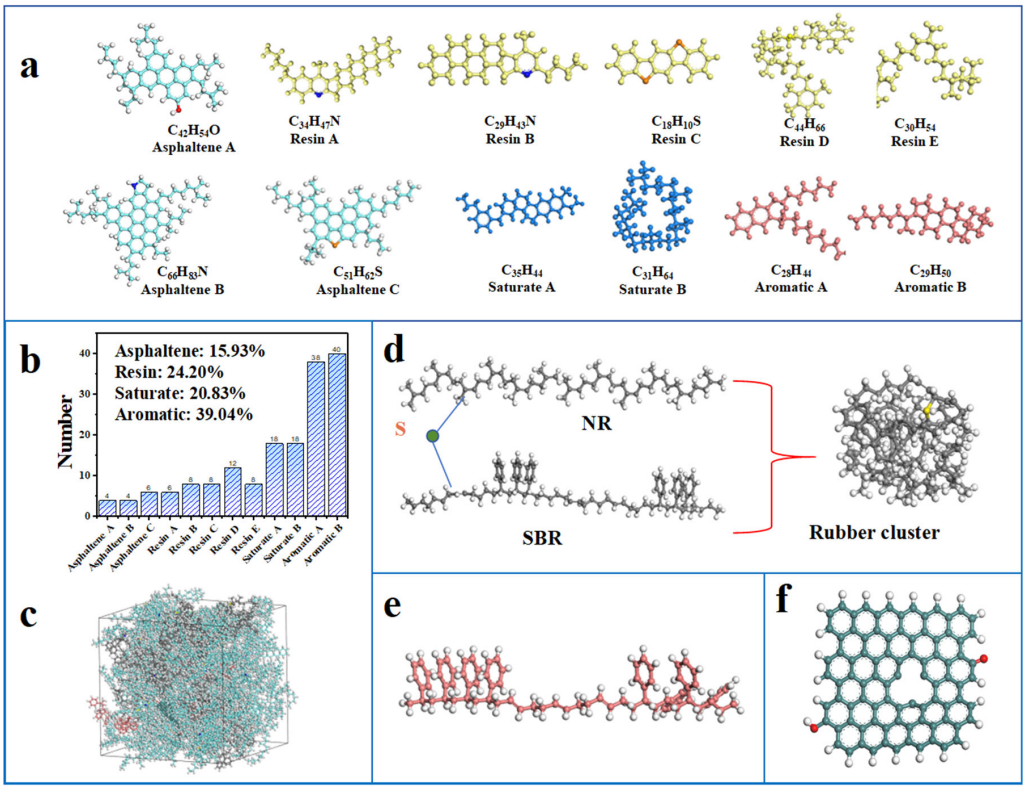


Figure 11. The model molecules were constructed: (**a**) twelve types of asphalt molecules, (**b**) the content ratios of the four asphalt components, (**c**) asphalt molecular model, (**d**) CR particles, (**e**) SBS, and (**f**) PG.

3.2. Simulation Process

The molecular dynamics simulation in this work was carried out using MS 2017 software. Asphalt is a mixture of organic molecules, so the COMPASS force field was used to calculate the properties of the asphalt molecular models [30]. The simulation steps were as follows: (1) each model was geometrically optimized until the energy of the model structure was minimized; (2) the model structure was annealed, heated from 200 K to 450 K, then cooled after reaching 450 K, with the system relaxed and energy minimized over five cycles to reach equilibrium; (3) the molecular dynamics simulation was run in the NVT ensemble for 1 ns at the set temperature with a time step of 0.5 fs, followed by the NPT ensemble at the set temperature and 0.1 MPa for 200,000 steps, with configurations output every 5000 steps. The NVT ensemble was controlled by the Nose thermostat and the NPT ensemble by the Berendsen barostat. The molecular dynamics simulations were carried out at 273 K and 353 K to investigate the mechanical properties of asphalt at high and low temperatures.

3.3. Stretching Process Simulation

The MS stress–strain scripting program was used to simulate the stress–strain response of PG composite SBS/CR-modified asphalt at a constant temperature and a constant strain rate of 5.0×10^9 s^{-1} to explore its mechanical properties at the molecular level. In this work, the model was stretched laterally in the NPT ensemble, and the pressures in the x and y directions were independently controlled using the Nosé–Hoover anisotropic barostat, allowing the simulation cell to expand or contract laterally due to the Poisson effect. Then, the molecular structure changes were analyzed from snapshots taken during the stretching process.

3.4. Shear Process Simulation

The Forcite module in MS software was employed to explore the mechanical properties of modified asphalt. First, 200,000-step MD simulations of the asphalt model were performed under NVT conditions at different temperatures, and then the energy of the asphalt system was calculated using the stiffness matrix and compliance matrices. A fixed strain of 0.003 was applied within the elastic limit to calculate the shear modulus of the modified asphalt.

3.5. Analysis of Asphalt Model Structure

The distribution of asphalt components has a significant impact on the microstructure. In this work, after obtaining the equilibrium configurations of the asphalt molecular models from molecular dynamics simulations, we calculated the following quantities: mean squared displacement (MSD), radius of gyration, free volume and binding energy. These quantities were used to evaluate the molecular diffusion, distribution pore volume and molecule binding ability of modified asphalt.

3.5.1. Diffusion Coefficient

The MDC is an important indicator of the mobility of asphalt molecules. It was obtained using the Forcite analysis module by calculating the MSD of the molecules during molecular dynamics simulations. According to Einstein's diffusion law, when the simulation time is sufficiently long, the MDC is one-sixth of the slope of the MSD curve [31].

3.5.2. Radius of Gyration

Rg is the radius of gyration of polymer chain segments rotating around their center of mass: it reflects the dynamic changes in the volume and shape of asphalt molecules and is used to assess their compactness [32].

3.5.3. Free Volume

The free volume of atoms in the asphalt model was calculated using Atom volume & Surface in MS. In this work, the position of the RDF peak of carbon atoms in the asphalt model was used as the probe size [33] to calculate the free volume of modified asphalt at a given temperature, in order to evaluate the motion of asphalt molecular chains or micelle units.

3.5.4. Binding Energy

In Materials Studio, the binding energy between components of a mixture is calculated from the thermodynamic definition: the binding energy equals the sum of the energies of the isolated components minus the total energy of the mixture. The formula is as follows:

$$E_{bind} = E_{componentA} + E_{componentB} - E_{total(A+B)} \quad (1)$$

where $E_{componentA}$ and $E_{componentB}$ are the single-point energies of components A and B at the same conformation or equilibrium state, respectively, and $E_{total(A+B)}$ is the total energy of the mixed system containing A and B. If the result is positive, it shows that there is attraction between the components, and the larger the value, the tighter the binding usually is; a negative value indicates repulsion or that the system is unstable.

4. Conclusions

This work used molecular dynamics simulations to reveal the mechanism underlying the enhanced properties of PG composite SBS/CR-modified asphalt at high and low temperature. The results showed that 2% PG yielded the best mechanical properties in

the blend system. At 353 K, the modulus of 2% G-SBS/CR MA was 30.8% higher than that of SBS/CR MA, and the total MDC decreased by 24.14%. At 273 K, the MDC of SBS in G/SBS/CR MA was 101.6% higher than in SBS/CR MA, confirming that 2% PG can effectively improve high-temperature elasticity and low-temperature flexibility. Molecular dynamics simulations also confirmed that at a 2% dosage, PG exhibited the strongest electrostatic adsorption with CR molecules. SBS molecules exhibited greater extensibility in the system, acting as bridges connecting CR molecules, effectively reducing the free volume in the modified asphalt blend, enhancing cohesion and viscosity, and improving high-temperature mechanical properties. In addition, PG effectively promoted the low-temperature diffusion of SBS, thereby improving the low-temperature crack resistance of the modified asphalt blend. Overall, this study demonstrates that the amount of PG is crucial for improving SBS/CR-modified asphalt and reveals the enhancement mechanism of PG composite SBS/CR-modified asphalt at high and low temperatures, providing theoretical support for the applied engineering of modified asphalt.

Author Contributions: Conceptualization, Y.H. and S.H.; methodology, Z.W.; software, W.J.; validation, Y.H., L.M. and Z.W.; formal analysis, Y.H.; investigation, H.W.; resources, Z.W.; data curation, W.J. and H.W.; writing—original draft preparation, Y.H.; writing—review and editing, S.H.; visualization, H.W.; supervision, L.M.; project administration, Y.H.; funding acquisition, Y.H. All authors have read and agreed to the published version of the manuscript.

Funding: This research was funded by the Guangxi Natural Science Foundation Youth Project, grant number 2026GXNSFBA00640370; Guangxi Science and Technology Program, Grant number ZG2503980029.

Institutional Review Board Statement: Not applicable.

Informed Consent Statement: Not applicable.

Data Availability Statement: The raw data supporting the conclusions of this article will be made available by the authors upon reasonable request.

Conflicts of Interest: The authors declare no conflicts of interest.

References

1. Ullah, Z.; Zhang, Z.; Liu, H.; Ji, J.; Li, Q.; Rukundo, S.P.; Bilal, M. Application of nanomaterials on the performance of SBS modified asphalt binders and mixtures: A comprehensive review. *J. Road Eng.* **2025**, *5*, 323–342. [CrossRef]
2. Araby, S.; Abdulhamid, A.; Bakhbergen, U.; Kim, J.; Abd-Elaal, E.-S. Advancements of carbon nanomaterials-modified asphalt: Processes, properties, economic feasibility and future perspectives. *J. Traffic Transp. Eng.* **2025**, *12*, 965–1010. [CrossRef]
3. Yang, S.; Liu, D.; Zhu, H.; Li, R.; Tan, Q.; Qi, A.; Xu, B.; Lv, H. Preparation and characterization of composite epoxy asphalt based on modified graphene oxide: Enhancements in toughness, thermal stability, and workability. *Case Stud. Constr. Mater.* **2026**, *24*, e05876. [CrossRef]
4. Liu, J.; Zuo, Y.; Lu, Y.; Huang, L.; Sun, B.; Guo, X. Comparative investigation on rheological, thermal, and healing properties of functionalized graphene-compounded polymer modified asphalt. *Case Stud. Constr. Mater.* **2026**, *24*, e06097. [CrossRef]
5. Guo, T.; Li, Z.; Chen, Y.; Xu, Q.; Wang, J.; Jin, L. Study on the performance and mechanism of graphene oxide/polyurethane composite modified asphalt. *Sci. Rep.* **2025**, *15*, 2482. [CrossRef]
6. Gao, Y.; Xie, Y.; Liao, M.; Li, Y.; Zhu, J.; Tian, W. Study on the mechanism of the effect of graphene on the rheological properties of rubber-modified asphalt based on size effect. *Constr. Build. Mater.* **2023**, *364*, 129815. [CrossRef]
7. Du, J.; Li, G.; Yan, K.; Zhao, X. Preparation and Performance Study of Thermoplastic Polyurethane/Graphene Oxide Modified Asphalt. *Materials* **2026**, *19*, 857. [CrossRef]
8. Shu, B.; Zeng, G.; Li, L.; Zhu, M.; Ma, Y. Study on the performance and mechanism of aging asphalt with organic–inorganic composite rejuvenator. *AIP Adv.* **2025**, *15*, 015026. [CrossRef]
9. Kabir, S.F.; Mousavi, M.; Fini, E.H. Selective adsorption of bio-oils' molecules onto rubber surface and its effects on stability of rubberized asphalt. *J. Clean. Prod.* **2020**, *252*, 119856. [CrossRef]
10. Zhang, S.; Yan, Y.; Yang, Y.; Guo, R. Study on the Physical and Rheological Characterisation of Low-Density Polyethylene (LDPE)/Recycled Crumb Rubber (RCR) on Asphalt Binders. *Molecules* **2024**, *29*, 716. [CrossRef]

11. Ren, S.; Liu, X.; Jing, R.; Gao, Y.; Lin, P.; Erkens, S. Investigating the rheological properties and compatibility behaviours of RET/PE and WR/CR/SBS compound-modified bitumen. *Road Mater. Pavement. Des.* **2024**, *25*, 653–677. [CrossRef]
12. Zhang, H.; Yu, J.; Wu, S. Effect of montmorillonite organic modification on ultraviolet aging properties of SBS modified bitumen. *Constr. Build. Mater.* **2012**, *27*, 553–559. [CrossRef]
13. Liu, Y.; Zheng, M.; Zhu, Y.; Zhu, L.; Li, H.; Liu, P. Preparation and performance of oxidized crumb rubber (OCR)/nano-SiO_2 composite-modified asphalt. *Constr. Build. Mater.* **2021**, *279*, 122488. [CrossRef]
14. Yang, J.; Muhammad, Y.; Yang, C.; Liu, Y.; Su, Z.; Wei, Y.; Li, J. Preparation of TiO_2/PS-rGO incorporated SBS modified asphalt with enhanced resistance against ultraviolet aging. *Constr. Build. Mater.* **2021**, *276*, 121461. [CrossRef]
15. Hussein, A.A.; Jaya, R.P.; Hassan, N.A.; Yaacob, H.; Huseien, G.F.; Ibrahim, M.H.W. Performance of nanoceramic powder on the chemical and physical properties of bitumen. *Constr. Build. Mater.* **2017**, *156*, 496–505. [CrossRef]
16. He, J.; Hu, W.; Xiao, R.; Wang, Y.; Polaczyk, P.; Huang, B. A review on Graphene/GNPs/GO modified asphalt. *Constr. Build. Mater.* **2022**, *330*, 127222. [CrossRef]
17. Li, X.-L.; Guo, J.-G.; Zhou, L.-J. The Young's modulus of triangle-like three-dimensional graphene under uniaxial tension: Finite element method and theoretical model. *J. Phys. Chem. Solids* **2022**, *161*, 110473. [CrossRef]
18. Marsden, A.J.; Skilbeck, M.; Healey, M.; Thomas, H.R.; Walker, M.; Edwards, R.S.; Garcia, N.A.; Vuković, F.; Jabraoui, H.; Walsh, T.R.; et al. From graphene to graphene oxide: The importance of extended topological defects. *Phys. Chem. Chem. Phys.* **2022**, *24*, 2318–2331. [CrossRef]
19. Li, B.; Liu, P.; Zhao, Y.; Li, X.; Cao, G. Effect of graphene oxide in different phases on the high temperature rheological properties of asphalt based on grey relational and principal component analysis. *Constr. Build. Mater.* **2023**, *362*, 129714. [CrossRef]
20. Wang, Y.; Polaczyk, P.; He, J.; Lu, H.; Xiao, R.; Huang, B. Dispersion, compatibility, and rheological properties of graphene-modified asphalt binders. *Constr. Build. Mater.* **2022**, *350*, 128886. [CrossRef]
21. Adnan, A.M.; Wang, J. Enhancement of rheological performance and compatibility of tire rubber-modified asphalt binder with the addition of graphene. *Constr. Build. Mater.* **2023**, *402*, 133038. [CrossRef]
22. Li, Z.; Guo, T.; Chen, Y.; Dong, L.; Chen, Q.; Hao, M.; Zhao, X.; Liu, J. Study on Rheological Properties of Graphene Oxide/Rubber Crowd Composite-Modified Asphalt. *Materials* **2022**, *15*, 6185. [CrossRef]
23. Chen, Y.; Huang, J.; Muhammad, Y.; Zhao, Z.; Fan, S.; Luo, W.; Li, J. Study on the performance and mechanism of carbon nanomaterials incorporated SBS composite modified asphalt. *Constr. Build. Mater.* **2023**, *389*, 131795. [CrossRef]
24. Shi, X.; Cao, L.N.Y.; Chen, M.; Huang, Y. Recent progress on two-dimensional materials confining single atoms for CO_2 photoreduction. *Chin. Chem. Lett.* **2022**, *33*, 5023–5029. [CrossRef]
25. Huo, S.; Chen, B.; Lei, Y. Research on the mechanism of graphene/rubber composite-modified asphalt based on molecular dynamics. *Arch. Civ. Eng.* **2026**, *72*, 169–184. [CrossRef]
26. Yeom, M.S. Concentration and Confinement Effects on the Behavior of Polymer Chains in Confined Channels by Dissipative Particle Dynamics Simulation. *J. Korean Phys. Soc.* **2008**, *52*, 56–63. [CrossRef]
27. Huang, Y.; Wu, Z.; Liang, L.; Ying, J.; Gui, L.; Shen, P.K.; Tian, Z. Revealing the dependance of mechanical properties of asphalt binder on graphene size via multi-scale methods. *Mater. Des.* **2023**, *236*, 112478. [CrossRef]
28. Huang, Y.; Wu, Z.; Liang, L.; Ying, J.; Gui, L.; Mo, L.; Shen, P.K.; Tian, Z. Critical role of vacancy defects in graphene nanosheets for enhancing asphalt binder. *Constr. Build. Mater.* **2024**, *438*, 137139. [CrossRef]
29. Xiong, H.; Liang, S.; Liu, Q.; Ren, S.; Pipintakos, G.; Wu, S.; Liu, M.; Xu, S. Experimental and molecular dynamics investigation of the rejuvenation effect of bio-oils on aged high-penetration asphalt. *Materials* **2025**, *18*, 5252. [CrossRef]
30. Liao, M.; Gao, Y.; Xie, Y.; Zhu, J.; Li, Z.; Tian, W.; Zhu, Z. Investigation on the anti-aging properties enhancement mechanism of graphene on RA based on size effect. *Case Stud. Constr. Mater.* **2022**, *17*, e01634. [CrossRef]
31. Ren, S.; Liu, X.; Zhang, Y.; Lin, P.; Apostolidis, P.; Erkens, S.; Li, M.; Xu, J. Multi-scale characterization of lignin modified bitumen using experimental and molecular dynamics simulation methods. *Constr. Build. Mater.* **2021**, *287*, 123058. [CrossRef]
32. Wu, Z.; Huang, Y.; Gui, L.; Liang, L.; Ying, J.; Li, W.; Shen, P.K.; Tian, Z. 3D porous graphene nanosheets as efficient additives for high-performance styrene-butadiene-styrene/crumb rubber blend-modified asphalt. *Mater. Des.* **2023**, *232*, 112157. [CrossRef]
33. Nie, F.; Chow, C.L.; Lau, D. Effect of functionalization and defects on thermal conductivity of graphene sheets modified asphalt nanocomposites. *Appl. Surf. Sci.* **2023**, *621*, 156804. [CrossRef]

Disclaimer/Publisher's Note: The statements, opinions and data contained in all publications are solely those of the individual author(s) and contributor(s) and not of MDPI and/or the editor(s). MDPI and/or the editor(s) disclaim responsibility for any injury to people or property resulting from any ideas, methods, instructions or products referred to in the content.